



Article

Selective Oxidation of Halophenols Catalyzed by an Artificial Miniaturized Peroxidase

Daniele D'Alonzo , Maria De Fenza , Vincenzo Pavone , Angela Lombardi and Flavia Nastri *

Department of Chemical Sciences, University of Napoli Federico II, Via Cintia, 80126 Napoli, Italy; dandalonzo@unina.it (D.D.); maria.defenza@unina.it (M.D.F.); vincenzo.pavone@unina.it (V.P.); alombard@unina.it (A.L.)

* Correspondence: flavia.nastri@unina.it; Tel.: +39-081-674-419

Abstract: The development of artificial enzymes for application in sustainable technologies, such as the transformation of environmental pollutants or biomass, is one of the most challenging goals in metalloenzyme design. In this work, we describe the oxidation of mono-, di-, tri- and penta-halogenated phenols catalyzed by the artificial metalloenzyme Fe-MC6*a. It promoted the dehalogenation of 4-fluorophenol into the corresponding 1,4-benzoquinone, while under the same experimental conditions, 4-chloro, 4-bromo and 4-iodophenol were selectively converted into higher molecular weight compounds. Analysis of the 4-chlorophenol oxidation products clarified that oligomers based on C-O bonds were exclusively formed in this case. All results show that Fe-MC6*a holds intriguing enzymatic properties, as it catalyzes halophenol oxidation with substrate-dependent chemoselectivity.

Keywords: artificial peroxidase; halophenols; miniaturization; metalloenzyme design; chemoselectivity



Citation: D'Alonzo, D.; De Fenza, M.; Pavone, V.; Lombardi, A.; Nastri, F. Selective Oxidation of Halophenols Catalyzed by an Artificial Miniaturized Peroxidase. *Int. J. Mol. Sci.* **2023**, *24*, 8058. <https://doi.org/10.3390/ijms24098058>

Academic Editor: Claudiu T. Supuran

Received: 27 March 2023

Revised: 24 April 2023

Accepted: 25 April 2023

Published: 29 April 2023



Copyright: © 2023 by the authors. Licensee MDPI, Basel, Switzerland. This article is an open access article distributed under the terms and conditions of the Creative Commons Attribution (CC BY) license (<https://creativecommons.org/licenses/by/4.0/>).

1. Introduction

Metalloenzymes are very important tools in catalysis, thanks to their huge functional diversity, unrivaled efficiency and high level of selectivity [1–4]. Given their evolution-driven ability to activate even inert molecules and to produce high-added-value chemicals under mild conditions, metalloenzymes are not only essential for metabolic functions, but they also have a role in a variety of research areas, including asymmetric synthesis, biosensing, synthetic biology and industrial microbiology [5]. The outstanding catalytic properties of metalloenzymes are the result of a complex and strong interplay between metal cofactors and protein scaffolds, mutually affecting enzymatic function and substrate selectivity [1,6]. Indeed, the protein matrix tunes the reactivity of metal ions through first and second sphere interactions while influencing substrate access owing to its inherently chiral environment [7]. Furthermore, in many cases the metal cofactor assists in protein folding, contributing to making the whole molecule catalytically functional [8].

Several metalloenzymes are, however, innately characterized by narrow substrate selectivity, as natural selection resulted in unique binding elements for specific enzymatic functions. The intricate network of non-covalent interactions necessary for protein folding and activity makes metalloenzymes highly sensitive to experimental reaction conditions [6]. After decades of efforts aimed at overcoming these limitations, researchers have now impressively enriched the catalytic toolbox by constructing artificial metalloenzymes [9,10]. Whether exploiting one of the numerous strategies [11,12], including but not limited to miniaturization [13], de novo design [14–18], rational design [19,20], directed evolution [21,22] or supramolecular assembly [23], minimal or more extensive changes to the protein scaffold and/or the metal cofactor have been conceived, enabling the development of new-to-nature architectures with enhanced features compared with native metalloenzymes. Several examples of designed and engineered metalloenzymes endowed with higher catalytic robustness, such as stability under operating conditions and tolerance

to non-aqueous solvents [24–26], a broader substrate specificity (even toward non-natural catalysis [27,28]) and more effective substrate selectivity [9,14] have been reported.

In this respect, an illustrative example has been provided by our long-studied family of miniaturized metalloenzymes called “mimochromes” (MCs) [4,12,13,29]. MCs have been demonstrated to combine remarkable stability, high catalytic potential and tunable enzymatic activity in a single molecule [4,11,29] by virtue of their minimal but finely designed peptide scaffold, involving two alpha-helical peptides covalently linked to a deuteroporphyrin core [30]. The latest and most promising member of this family, MC6*a, is an excellent and versatile catalyst. Its enzymatic activity significantly depends on the nature of the metal ion (Figure 1). The metalloenzyme housing cobalt ion into the porphyrin (Co-MC6*a) acts as a promising catalyst for hydrogen-evolution reactions either in electrocatalytic or photochemical systems [31–33] (Figure 1a). The manganese derivative of MC6*a (Mn-MC6*a) represents an efficient peroxygenase, performing highly selective oxidative transformations, such as the sulfoxidation of aryl thioethers [34]. Furthermore, in the model reaction of indole oxidation, Mn-MC6*a is able to oxidize the substrate with unprecedented pH-dependent regioselectivity, providing unnatural chemicals with high synthetic utility [35] (Figure 1b). The iron-containing derivative, Fe-MC6*a, mainly acts as a peroxidase model, with intriguing catalytic properties in the oxidation of various substrates [36,37]. When assayed in the dehalogenation reaction of the pollutant 2,4,6-trichlorophenol (TCP), Fe-MC6*a exhibited the highest catalytic efficiency among both natural and artificial metalloenzymes, tested in the same reaction [38] (Figure 1c).

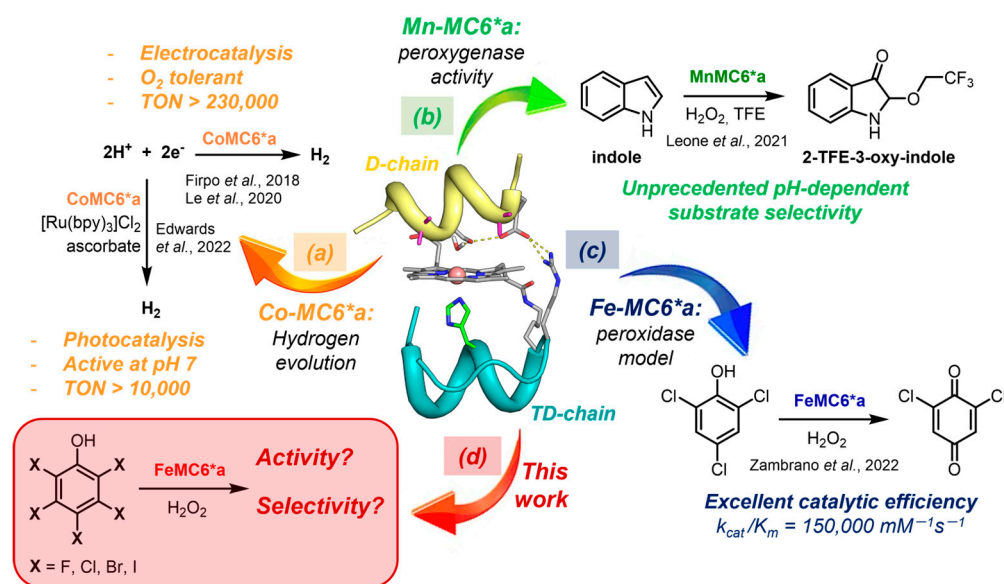


Figure 1. Molecular model of the MC6*a scaffold, with indications of its catalytic potential. The two peptide chains are depicted in different colors: tetradecapeptide (TD) in cyan and decapeptide (D) in yellow. The corresponding sequences are: TD chain, Ac-D-L-Q-Q-L-H-S-Q-K-R-K-I-T-L-NH₂; D-chain, Ac-D-E-U-Q-L-S-U-Q-K-R-NH₂. (a) Catalytic properties of Co-MC6*a in hydrogen evolution reaction [31–33]; (b) peroxygenase activity of Mn-MC6*a in indole oxidation [35]; (c) catalytic potential of Fe-MC6*a in TCP oxidation [38]; (d) this work: evaluation of the activity and selectivity of Fe-MC6*a in the oxidation of variously halogenated phenols. Adapted with permission from Ref. [11], 2019, Elsevier.

The excellent behavior of Fe-MC6*a in TCP dehalogenation [38] encouraged us to carry out a more extensive evaluation of its reactivity toward a variety of other halogenated phenols, including mono-, di-, tri- and penta-halophenols (Figure 1d). Halophenols represent interesting substrates for oxidative catalysis. Due to their well-known toxicity [39], their biocatalytic degradation is a highly demanding task in view of prospective applications in environmental biotechnologies [20]. Furthermore, several halophenols represent key

components in many pharmaceuticals, and they are used in diverse therapeutic areas [40] (Figure 2). Thus, their selective conversion into higher reactivity synthons may result in being very useful for drug synthesis.

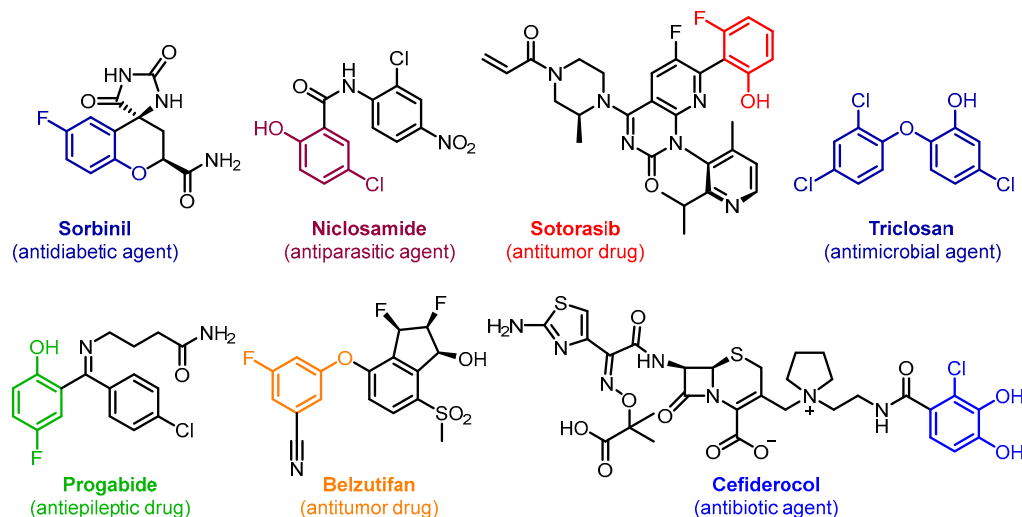


Figure 2. Representative examples of pharmaceuticals containing halophenols and their derivatives. Halophenol moieties are highlighted in different colors.

A plethora of biocatalytic halophenol oxidation reactions by both natural and artificial heme-enzymes has been reported in the literature, involving peroxidases [41], globins [42], globin-like enzymes [43] and oxygenases [44]. However, in many cases, low or no selectivity has been associated to these reactions [45–47], thus making these biocatalysts of limited interest from a synthetic standpoint. Herein, we report that Fe-MC6*a promotes the efficient oxidation of various halophenols while enabling highly selective transformations, whose fate depends on the nature of the halogen atom. The intriguing enzymatic behavior of Fe-MC6*a further broadens the catalytic potential of this artificial metalloenzyme to produce synthetically useful building blocks and the degradation of organic pollutants.

2. Results and Discussion

2.1. H_2O_2 -Dependent Dehalogenation Activity of Fe(III)-MC6*a

The catalytic activity of Fe-MC6*a toward the H_2O_2 -dependent dehalogenation was first screened on differently substituted halophenols, including mono-, di-, tri- and penta-halophenols, by evaluating the turnover number (TON) [48]. All reactions were performed using the same procedure, with small changes depending on the nature of the substrate. Under typical reaction conditions, H_2O_2 was added to a stirring mixture of the given halophenol and Fe-MC6*a, dissolved in a 50 mM phosphate buffer (pH 6.5) solution containing 2,2,2-trifluoroethanol (TFE) as a cosolvent (50% *v/v*). After 30 min stirring at room temperature, the reaction was quenched and the mixture analyzed by GC-MS. TON values were determined by measuring the conversion degree based on the substrate consumption, compared to the peak area associated to methyl phenyl sulfone (MPS), used as an internal standard (Table 1).

Table 1. TON values of the Fe-MC6*a-catalyzed oxidation of halophenols.

Entry	Substrate	Abbreviation	TON
1	2-Chlorophenol	2-CP	310 ± 19
2	4-Fluorophenol ¹	4-FP	503 ± 10
3	4-Chlorophenol	4-CP	325 ± 22
4	4-Bromophenol	4-BP	235 ± 10
5	4-Iodophenol	4-IP	208 ± 30
6	2,4-Dichlorophenol ²	2,4-DCP	2588 ± 103
7	2,4,6-Trifluorophenol ²	2,4,6-TFP	3825 ± 171
8	2,4,6-Trichlorophenol ²	2,4,6-TCP	3850 ± 148
9	Pentafluorophenol	PFP	142 ± 27
10	Pentachlorophenol	PCP	186 ± 64

General conditions: [Fe-MC6*a] = 6.25×10^{-3} mM; [substrate] = 2.5 mM; [H₂O₂] = 2.5 mM; 50 mM phosphate buffer, pH 6.5 with 50% (v/v) TFE. MPS was used as an internal standard ([MPS] = 2.5 mM). ¹ In this case, [4-FP] = [H₂O₂] = 3.75 mM; the remaining parameters were left unchanged. ² In this case, [Fe-MC6*a] = 6.25×10^{-5} mM, while the remaining parameters were left unchanged.

The position of halogen did not affect TON values. As an example, TONs for the Fe-MC6*a-catalyzed oxidations of 2-chlorophenol (2-CP) and 4-chlorophenol (4-CP) were reasonably similar, as they varied between 310 (2-CP oxidation; entry 1) and 325 (4-CP oxidation; entry 3). Furthermore, the conversion degrees were slightly influenced by the nature of the halogen atom in the substrate, with a progressive decrease in the TON values when the oxidation reaction involved 4-fluorophenol (4-FP, 503 TONs; entry 2), 4-CP (325 TONs; entry 3), 4-bromophenol (4-BP, 235 TONs; entry 4) and 4-iodophenol (4-IP, 208 TONs; entry 5) as substrates. In contrast, the TONs varied dramatically along with the substrate halogenation degree. Indeed, the TON value that referred to the Fe-MC6*a-catalyzed conversion of 4-CP was 325 (entry 3), whereas the reaction with 2,4-dichlorophenol (2,4-DCP) proceeded with a TON value of 2588 (entry 6). As already reported [38], in the case of 2,4,6-trichlorophenol (2,4,6-TCP), the TON value further increased up to 3850 (entry 8). Similarly, the TON that referred to the reaction of 2,4,6-trifluorophenol (2,4,6-TFP) was 3825 (entry 7). Conversely, the oxidations of 2,3,4,5,6-pentafluorophenol (PFP) and 2,3,4,5,6-pentachlorophenol (PCP) were associated with TON values of only 142 and 186, respectively (entries 9 and 10). The observed low TONs for these two substrates could be due to their steric hindrance when approaching the catalytically active Compound I (Cpd I).

2.2. Outcome of the Reaction: Case Study of 4-Halophenols

A deep investigation of the nature of the conversion products and their distribution was then carried out. To this end, the Fe-MC6*a-catalyzed dehalogenation reaction involving 4-halophenols was selected as a case study.

2.2.1. Benzoquinone Formation in 4-Fluorophenol Conversion

The reaction of Fe-MC6*a with H₂O₂ and 4-FP was monitored by UV-Vis spectroscopy (Figure 3). Upon H₂O₂ addition, a rapid decrease in the 4-FP absorption maximum (275 nm) was observed (Figure 3), while a concurrent increase of bands at 245 and 301 nm, characteristic of 1,4-benzoquinone (BQ), was detected. No reaction progress over the same timescales was observed in the absence of the catalyst.

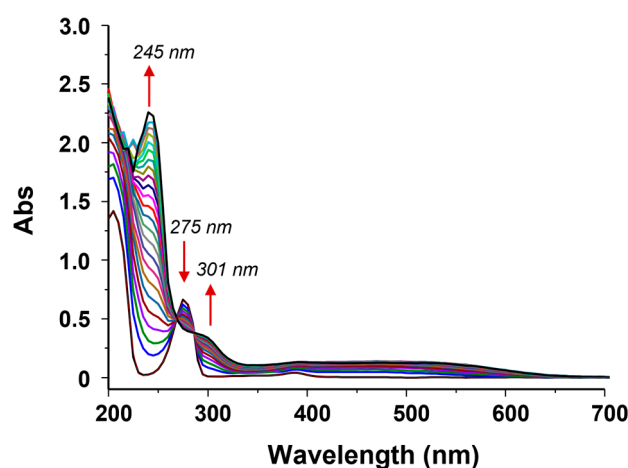


Figure 3. Time-dependent UV-Vis spectra (acquired over 100 min) of Fe(III)-MC6*a (6.25×10^{-4} mM) in the presence of 4-FP (0.25 mM) in 50 mM sodium phosphate (pH 6.5) with 50% TFE (*v/v*) upon addition of H₂O₂ (0.25 mM). Brown line, *t* = 0 min; black line, 100 min; spectra taken every 5 min are reported in different colors.

Analysis of the crude mixture for the catalyzed reaction by UHPLC confirmed the formation of a single reaction product (Figure 4).

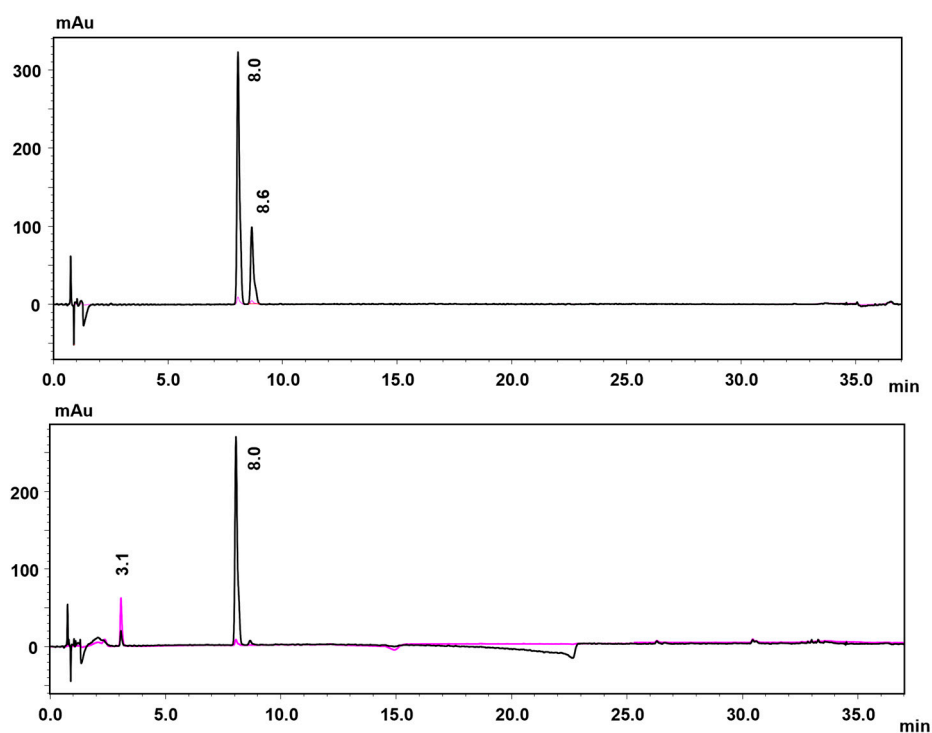
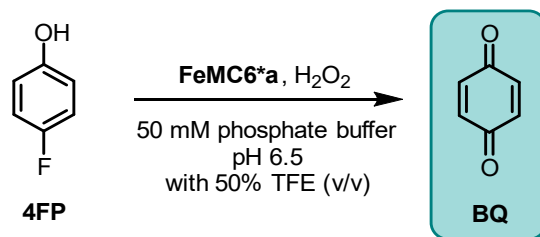


Figure 4. UHPLC traces (black line: $\lambda = 220$ nm, pink line: $\lambda = 240$ nm) of the Fe-MC6*a-catalyzed oxidation of 4-FP before (upper trace) and 30 min after (lower trace) H₂O₂ addition. Reaction conditions: [Fe-MC6*a] = 6.25×10^{-3} mM; [4-FP] = 2.5 mM; [H₂O₂] = 2.5 mM; phosphate buffer (50 mM) at pH 6.5 with 50% TFE (*v/v*). The peak with *Rt* = 8.0 min is MPS, used as internal standard.

Within 30 min of the reaction, a complete conversion of 4-FP (*Rt* = 8.6 min) into a single oxidation product (*Rt* = 3.1 min) was observed (Figure 4). The identification of the reaction product was accomplished after extraction of the reaction mixture. A GC-MS analysis of the extracted sample confirmed the formation of BQ as the main dehalogenation product (Scheme 1) because of the presence of a main peak at *m/z* 108 ($[M]^+$; see Figure S1).

Further confirmation of the nature of the oxidation product was provided by analyzing a commercial sample of BQ under the same chromatographic conditions.



Scheme 1. Oxidative defluorination of 4-FP.

It is worth underlining that the outcome of this reaction was significantly different from those observed with most heme-containing metalloenzymes, assayed in the same reaction. Horseradish peroxidase (HRP) and Chloroperoxidase from *Caldariomyces fumago* (CCPO) are reported to provide, along with variable amounts of BQ, coupling products based on unsymmetrical pairing of 4-fluorophenol radicals [46,47]. Low catalytic activity was documented for dehaloperoxidase from *Amphitrite ornata* (DHP-A), as both 4-FP and all the remaining 4-halophenols act as inhibitors based on internal binding [20,49–51], 4-FP being the weakest binder of the series. On the other hand, the aerobic oxidation of 4-FP catalyzed by cytochrome P450 (from rat liver microsomes) [52] and its mutants [53] provided 1,4-hydroquinone (HQ) as the reaction product, resulting from the reduction of BQ by NADPH-cytochrome P450 reductase. Our result is rather in line with the H_2O_2 -mediated oxidation reaction performed by another mini-enzyme, the cytochrome c-derived microperoxidase Fe^{III} -MP-8, which also converted 4-FP (as well as all other 4-halophenols) into benzoquinone [54] with comparable selectivity.

2.2.2. Coupling Products in 4-Chlorophenol Conversion

The analysis of the reaction products for the Fe-MC6^{*}-catalyzed oxidation of 4-CP turned out to be more challenging. Differently from 4-FP, the UV-Vis spectroscopic analysis of the reaction mixture using 4-CP as a substrate displayed a substantial increase in the intensity of all absorption bands of the starting material (Figure 5), likely suggesting the formation of products structurally similar to the reagent.

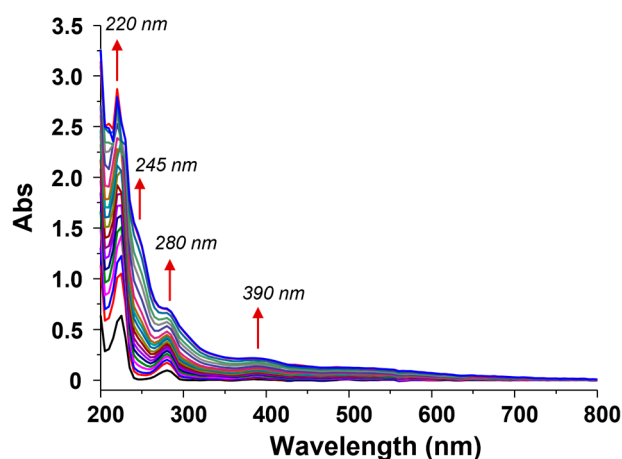


Figure 5. Time-dependent UV-Vis spectra (acquired over 100 min) of Fe(III)-MC6^{*}a (6.25×10^{-4} mM) in the presence of 4CP (0.25 mM) in 50 mM sodium phosphate (pH 6.5) with 50% TFE (*v/v*) upon H_2O_2 addition (0.25 mM). Black line, $t = 0$ min; red line, 100 min; spectra taken every 5 min are reported in different colors.

The ^1H NMR analysis of the reaction mixture ($[\text{Fe-MC6}^*a] = 6.25 \times 10^{-3}$ mM, $[\text{4-CP}] = 2.5$ mM, and $[\text{H}_2\text{O}_2] = 2.5$ mM) (Figure S2) showed a substantial decrease in the in-

tensity of the signals referring to 4-CP (doublets at 6.79 and 7.16 ppm) and a concurrent formation of one main signal at 6.76 ppm, related to BQ, whose intensity was, however, only approximately 5% compared to the starting 4-CP. This finding, together with the observed opalescence of the reaction mixture, suggests the formation of insoluble reaction products.

Upon removal of the insoluble portion by filtration, an analysis of the reaction mixture by UHPLC after 30 min from H₂O₂ addition indicated the conversion of 4-CP (Rt = 14.1 min, Figure 6, upper trace) into a very low amount of BQ (Rt = 3.1 min, Figure 6 lower trace). In contrast, two products with higher retention times with respect to 4-CP (Rt = 21.8 min and 29.3 min, Figure 6 lower trace) were observed.

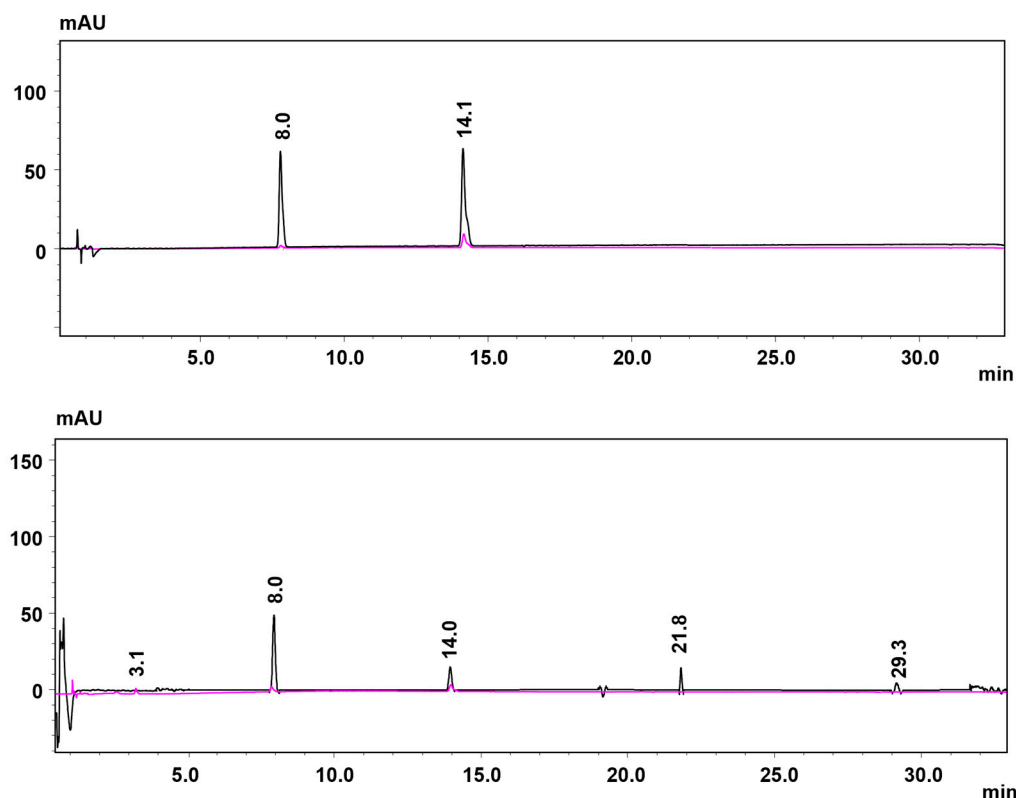
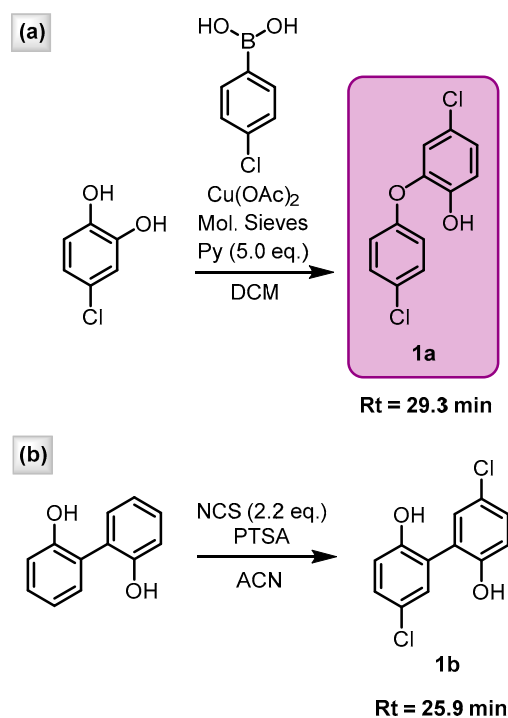


Figure 6. UHPLC traces (black line: $\lambda = 220$ nm; pink line: $\lambda = 240$ nm) of the Fe-MC6*a-catalyzed oxidation of 4-CP before (upper trace) and 30 min after (lower trace) H₂O₂ addition. *Reaction conditions:* [Fe-MC6*a] = 1.0×10^{-3} mM; [4-CP] = 2.5 mM; [H₂O₂] = 2.5 mM; [MPS] = 2.5 mM; phosphate buffer (50 mM) at pH 6.5 with 50% TFE (*v/v*). MPS (peak at Rt = 8.0 min) was used as an internal standard.

The UV-Vis spectral profile of the two main peaks related to 4-CP oxidation are similar to 4-CP (Figure S3), showing absorption maxima at λ values ($\lambda_1 = 211$ – 212 nm, $\lambda_2 = 293$ – 295 nm) close to those reported for 4-CP ($\lambda = 226$ nm, $\lambda = 280$ nm). An LC-ESI-MS analysis of the reaction mixture (negative ion mode) provided MS profiles compatible with 4-CP dimerization and trimerization products. In particular, the peak at Rt = 29.3 min shows a molecular ion peak at $m/z = 253.3$, [M-H][−], whereas the peak at Rt = 21.8 min corresponds to a species with $m/z = 379.2$, [M-H][−] (Figures S4 and S5). The additional identification of isotopic peaks at [M-H+2n][−] ($n = 1$ – 3) both represent a strong indication of the presence in the molecules of multiple chlorine atoms and excluded that a dehalogenation reaction had taken place in these cases.

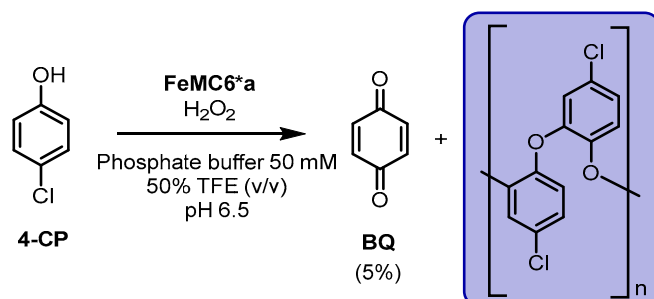
To unequivocally identify whether dimeric and trimeric products, obtained by the Fe-MC6*a-catalyzed 4-CP oxidation, involved C-C or C-O covalent bonds, the corresponding 4-chlorophenol C-C and C-O dimers were synthesized by literature procedures (Scheme 2). 4-Chloro-2-(4-chlorophenoxy)phenol (**1a**, Scheme 2a) was obtained using the

Evans method, relying on the copper(II)-promoted cross-coupling of 4-chlorophenylboronic acid and 4-chlorocatechol [55]. On the other hand, 5,5'-dichloro-[1,1'-biphenyl]-2,2'-diol (**1b**, Scheme 2b) was prepared using a slight variation of the synthetic method by Bentley et al. [56] (see Section 3 for the synthetic details). Figures S6–S8 report the NMR spectra of compounds **1a** and **1b**.



Scheme 2. Synthesis and UHPLC Rt values of 4-chloro-2-(4-chlorophenoxy)phenol (**1a**) and 5,5'-dichloro-[1,1'-biphenyl]-2,2'-diol (**1b**).

The UHPLC analysis of compounds **1a** and **1b** (Scheme 2 and Figure S9) provided peaks at Rt values of 29.3 min and 25.9 min, respectively. This allowed to identify the peak at Rt = 29.3 min, derived from the Fe-MC6*a-catalyzed oxidation of 4-CP, as the dimeric 4-CP coupling product based on a C-O bond. Furthermore, the absence in the UHPLC reaction profile of the peak at Rt = 25.9 min, corresponding to the C-C dimer (Scheme 2, compound **1b**), indirectly suggests that the trimeric species was also based on C-O bonds (Scheme 3).



Scheme 3. Reaction products in the Fe-MC6*a-catalyzed 4-CP oxidation.

The formation of self-coupling products among 4-CP units recalls the peroxidase activity of horse heart myoglobin, which has been reported to catalyze the H₂O₂-dependent dimerization of 4-CP under conditions representative of oxidative stress [42]. In this case, the dimeric species was revealed to be based on a C-C bond in *ortho* positions to the

OH groups. CCPO from *Caldariomyces fumago* and DHP from *Amphitrite ornata* were also described to provide a C-C-linked 4-CP dimer, along with variable amounts of BQ [45,57].

Having ascertained that the Fe-MC6^a-catalyzed 4-CP oxidation followed a different reaction route than 4-FP, an analysis of the reaction products was also carried out on 4-BP and 4-IP as substrates. As with 4-CP, with these substrates coupling products were observed, even though a lower conversion and a higher selectivity was found, as no traces of BQ were detected (Figures S10 and S11).

2.2.3. Identification of the Insoluble Products in the Fe-MC6^a-Catalyzed 4-CP Oxidation

Having identified dimeric and trimeric coupling products occurring in the soluble fraction of the 4-CP oxidation reaction mixture, MALDI analysis (positive ion mode) then enabled us to suggest the nature of the insoluble material formed in the reaction. A family of oligomers, including up to fourteen 4-CP units and one terminal BQ moiety, was evidenced in the MALDI-MS spectrum (m/z 1914, $[M + H]^+$; 1936, $[M + Na]^+$; Figure S12).

These structures are in agreement with a previous hypothesis provided by other authors and referring to peroxidase-promoted halophenol polymerization [58]. A subsequent FT-IR analysis (ATR mode) of the insoluble products (Figure 7, red line) provided further support to the formation of oligomers based on C-O bonds. The presence in the spectrum of bands at $\approx 800\text{ cm}^{-1}$ is diagnostic of the occurrence of C-Cl bonds in the polymer structure. Furthermore, broad bands at approximately 3300 cm^{-1} , typically referring to OH groups in phenols and in 4-CP, were missing. Finally, the minimal presence of bands at approximately 1700 cm^{-1} (compatible with CO bond stretching vibrations from benzoquinone moieties [59]) support the hypothesis of a “capping” reaction of the 4-CP oligomers, involving the dehalogenative oxidation of terminal 4-CP moieties to quinones.

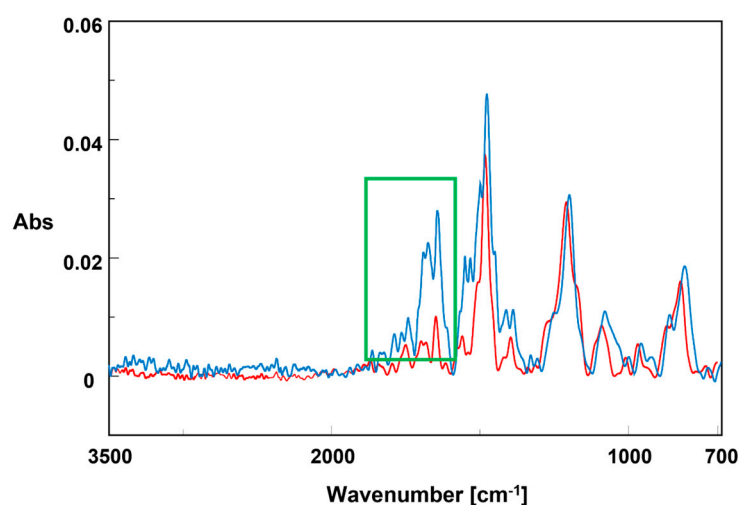


Figure 7. Comparison of FT-IR spectra referring to 4-CP polymerization resulting from Fe-MC6^a catalysis (red spectrum) or HRP catalysis (light-blue spectrum). The most relevant differences in the two spectra are highlighted in the green square.

It is well known that HRP is able to promote the H₂O₂-mediated polymerization of phenols and their derivatives, including 4-CP, providing insoluble products, based on a mixture of phenylene (C-C) and oxyphenylene (C-O) units [60–62]. This finding has been at the core of numerous research projects aimed at defining a protocol for the removal of 4-CP and other pollutants from wastewater [63–65]. To compare the regioselectivity of our artificial metalloenzyme with that of the HRP-catalyzed reaction, the conversion of 4-CP catalyzed by HRP was carried out, using optimal working conditions for the natural enzyme ($[HRP] = 1.0 \times 10^{-3}\text{ mM}$, $[4CP] = 2.5\text{ mM}$, $[H_2O_2] = 2.5\text{ mM}$, phosphate buffer 100 mM, and pH 6) [66]. An FT-IR analysis of the insoluble residue obtained in this reaction is reported in Figure 7 (light-blue line). Similar to the Fe-MC6^a-catalyzed reaction, bands at

$\approx 800\text{ cm}^{-1}$, referring to C-Cl bond stretching vibrations, were detected. Bands at 3300 cm^{-1} (OH bond stretching) were also absent in this case. Differently from the product obtained by Fe-MC6*a catalysis, herein larger and more intense bands ranging from 1800 to 1600 cm^{-1} were detected (Figure 7, light-blue line).

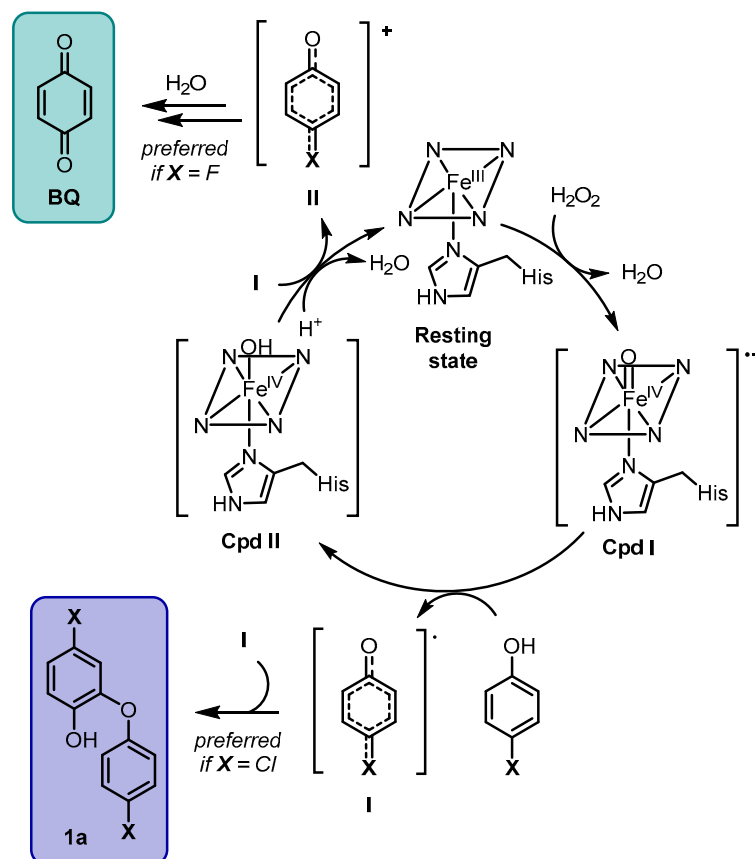
Thus, a comparison of the FT-IR spectra of the insoluble products obtained from the two different catalysts highlighted several common features but also some remarkable differences. The observation that the IR spectrum of the Fe-MC6*a catalysis product was characterized by the absence of phenolic groups with a minimal presence of quinone moieties suggests that the artificial enzyme is able to promote selective transformations, leading to polymerization products having high structural homogeneity. Conversely, in the case of HRP, the presence of intense bands referring to C=O bond stretching (Figure 7, green square) along with those dealing with C-Cl bond stretching suggests that the polymerization products, characterized by a higher structural diversity, were formed, resulting from both self-coupling and dehalogenative oxidation reactions. Furthermore, the absence of bands referring to OH groups' stretching vibrations suggests that side oxidation reactions of underivatized OH groups into quinones occurred.

2.3. Fe-MC6*a Chemodivergent Transformations in the Oxidation of Halophenols

The results presented above show that Fe-MC6*a catalysis exhibits peculiar features among both natural and artificial metalloenzymes. While peroxidases (HRP and CCPO) promote 4-halophenol oxidation leading to mixtures of both BQ and various radical-promoted coupling products (composed of both C-O and C-C bonds) independently from halogen's nature, the globin-like peroxidase DHP has a limited effect on 4-FP and 4-CP. Further, myoglobin (Mb) is able to transform 4-CP into a mixture of BQ and the C-C-linked 4-CP dimer. Among simplified metalloenzymes, MP8 enables the conversion of all 4-halophenols into BQ. In this scenario, Fe-MC6*a demonstrated the ability to promote substrate-dependent chemodivergent transformations, selectively providing BQ from 4-FP and coupling products from 4-CP. Additionally, in the latter case, catalysis provided oligomerization products based on C-O rather than C-C bonds, which were provided with unprecedented regioselectivity. The detection of oligomerization products is an indication that the reaction proceeds through the formation of radical species, as previously suggested by Dawson and coworkers [45]. In an effort to detect the 4-chlorophenoxy radical, 4-CP oxidation was performed in the presence of the radical scavenger DMPO (5,5-dimethyl-1-pyrroline-*N*-oxide) [67] and monitored by GC-MS analysis (Figures S13 and S14). While in the FeMC6*a-catalyzed 4-CP oxidation a significant substrate consumption was detected (Figure S13), the same reaction was totally inhibited when carried out in the presence of a large excess of DMPO (50 eq.; Figure S14).

Based on the above analysis of the product distribution obtained during the Fe-MC6*a-catalyzed oxidation of 4-halophenols, some preliminary mechanistic considerations may be proposed. First, the formation of oligomeric products is consistent with the involvement of radicals formed during the reaction. Second, the chemodivergent outcome of the reactions suggests that different substrates must have followed different oxidation routes. According to known mechanistic studies on natural metalloenzymes [44,45], as well as on the latest findings on the Fe-MC6*a-catalyzed oxidation of halophenols [38], the most plausible reaction mechanism for the Fe-MC6*a-catalyzed 4-halophenol oxidation (Scheme 4) involves the initial formation of Cpd I, characterized by the presence of an oxoferryl radical cation [(Fe(IV)=O)por⁺]. This intermediate species is obtained upon H₂O₂ activation of the catalyst in the resting state. Cpd I formation of Fe-MC6*a has already been demonstrated previously by spectroscopic studies [36,38]. Cpd I is thought to promote a one-electron oxidation, providing the phenoxy radical species I and Compound II (Cpd II), corresponding to the ferryl heme lacking the porphyrin radical, whose formation was postulated in previous studies [38]. Self-coupling reactions among radicals I are expected to provide dimer 1a and the corresponding oligomers. On the other hand, a further

one-electron oxidation from **I** yields a positively charged dienone **II**, which is converted into BQ upon reaction with a water molecule (Scheme 4).



Scheme 4. Fe-MC6*a chemodivergent catalysis with 4-halophenols.

Based on this catalytic cycle, we reasoned that the conversion of radical **I** into cation **II** represents the key step affecting the chemodivergent outcome of the reaction. Indeed, the accumulation of radical **I** is expected to favor the formation of self-coupling products, while the access to a higher concentration of **II** would enable the selective conversion of the 4-halophenol into BQ (Scheme 4). A suitable enzyme-driven accumulation of one of the two chemical species can be hypothesized to have a role in the product distribution of this reaction. Considering the uncatalyzed reaction, the formation of cation **II** is thermodynamically favored only in the reaction of 4-FP, owing to the more effective fluorine-mediated delocalization of the positive charge by electron-donating resonance effect. Conversely, no preference for radical **I** or cation **II** is expected when 4-CP, 4-BP and 4-IP are used as substrates. In the enzyme-catalyzed reaction, the preferential accumulation of single intermediates may occur, thus overcoming the stereoelectronic features of each substrate. This would imply the enzyme's ability to stabilize one chemical species over another one. More mechanistic studies will be performed to shed light on the molecular basis for the different pathways observed, aiming at establishing the role of our artificial catalyst over all existing metalloenzymes used for the same catalytic purposes.

3. Materials and Methods

All solvents were supplied by Romil (Cambridge, UK). All reagents including halophenols, MPS, 2,2'-biphenol, *p*-toluenesulfonic acid (PTSA), *N*-chlorosuccinimide (NCS), 4-chlorocatechol, 4-chlorophenylboronic acid, hydrogen peroxide (H₂O₂) solution (30% (*v/v*)), α -cyano-4-hydroxycinnamic acid (α -CHCA) and phosphate salts (mono- and dibasic) were purchased from Merck (Merck KGaA, Darmstadt, Germany). Fe(III)-MC6*a was synthesized, purified and characterized as previously described [36].

UV–Vis spectra were recorded on a Cary Varian 60 Probe UV spectrophotometer equipped with a temperature controller (Varian, Palo Alto, CA, USA). All measurements were performed at 25 °C in 50 mM phosphate buffer (pH 6.5) with 50% TFE (*v/v*), unless otherwise specified. Quartz cuvettes with a path length of 1.0 cm were used for the measurements. The wavelength scans were performed from 200 to 800 nm, with a 600 nm min⁻¹ scan speed. All data were blank subtracted. The Fe(III)-MC6*a concentration was determined by UV–Vis spectroscopy using $\epsilon = 1.17 \times 10^5 \text{ M}^{-1} \text{ cm}^{-1}$ in H₂O 0.1% TFA (*v/v*) ($\lambda = 387 \text{ nm}$). The data analysis was performed using Origin Pro, version 9.0 (Origin Lab Corporation, Northampton, MA, USA).

HPLC analyses were performed with a Shimadzu LC-20ADxr equipped with an SPDMS20A diode-array detector (Shimadzu Corporation, Kyoto, Japan). ESI-MS spectra were recorded on a Shimadzu LCMS-8040 system with ESI interface, triple-quadrupole mass analyzer (Shimadzu Corporation, Kyoto, Japan) and Shimadzu LC-MS solution Workstation (version 5.97) software for data processing. All analyses were performed with a Kinetex Phenyl-Hexyl column (150 mm \times 4.6 mm, 5 μm) using water with 0.1% TFA (A) and acetonitrile with 0.1% TFA (B) as the eluents. A linear gradient from 5 to 95% B over 35 min at a flow rate of 1.85 mL/min was used as the elution method.

GC-MS analysis was performed on a Shimadzu GCMS-QP2010 SE system equipped with an EI-MS source, a quadrupole array as an MS analyzer (Shimadzu Corporation, Kyoto, Japan) and a Shimadzu GC-MS solution Workstation (version 4.20) for data processing. A Restek Rxi-5Sil-MS column was used, with helium being selected as the carrier gas. A linear gradient from 50 °C to 300 °C with a rate of 24 °C·min⁻¹ was used. The mass spectra were recorded in an *m/z* range between 50 and 450.

Matrix-assisted laser desorption/ionization (MALDI)-MS experiments were performed on a 5800 MALDI time-of-flight (TOF)/TOF AB SCIEX equipped with a nitrogen laser (337 nm) (SCIEX, Framingham, MA, USA). The laser power was set to 3500 V for MS spectra acquisition. Each spectrum represents the sum of 10,000 laser pulses from randomly chosen spots per sample position. The data are reported as monoisotopic masses.

NMR spectra were acquired using Bruker Avance 600 or 400 MHz spectrometers (Karlsruhe, Germany). All NMR experiments were carried out at 298 K. All spectra were processed with MestreNova (version 14.2.2).

FT-IR-ATR spectra were recorded on solid phase by a JASCO FT/IR–430 spectrophotometer (JASCO Europe, Lecco, Italy) in the 4000–700 cm⁻¹ range, using HATR crystal zinc selenide (Flat Plate, PN 022–2020–45) by PIKE Technologies. The resolution was 2 cm⁻¹. Each spectrum was recorded 128 times.

3.1. Fe-MC6*a-Catalyzed Oxidations of Halophenols: General Procedure

For UV–Vis analysis: a solution of H₂O₂ (0.25 mM) was added in one portion at room temperature to a stirring solution of the halophenol (0.25 mM) and Fe(III)-MC6*a ($6.35 \times 10^{-4} \text{ mM}$) in 50 mM sodium phosphate (pH 6.5) with TFE (1:1 *v/v*). The reaction was carried out in an overall reaction volume of 0.66 mL. The reaction monitoring was performed by acquiring UV–Vis spectra over 100 min (wavelength window: 200–800 nm; scan speed: 600 nm/min).

For chromatographic analysis: a solution of H₂O₂ (2.5 or 3.75 mM) was added in one portion at room temperature to a stirring solution of the halophenol (2.5 or 3.75 mM), MPS (2.5 or 3.75 mM) and Fe(III)-MC6*a ($6.25 \times 10^{-3} \text{ mM}$ or $6.25 \times 10^{-5} \text{ mM}$) in 50 mM sodium phosphate (pH 6.5) with TFE (1:1 *v/v*). The reaction was carried out in an overall reaction volume of 1 mL. For GC-MS analysis, 50 μL aliquots were withdrawn before (*t* = 0) and after (*t* = 10, 20 and 30 min) H₂O₂ addition and transferred to 2.0 mL Eppendorf tubes. The reaction mixtures were quenched by the addition of a H₂O 0.1% TFA (*v/v*) (50 μL) and extracted with dichloromethane (100 μL). Organic layers were dried (Na₂SO₄), centrifuged at 4000 rpm and the supernatants were injected. For HPLC analysis, 50 μL aliquots were withdrawn before (*t* = 0) and after (*t* = 10, 20 and 30 min) H₂O₂ addition and transferred to

1.5 mL Eppendorf tubes. The reaction mixtures were quenched by the addition of a H₂O 0.1% TFA (*v/v*) (50 µL) and injected.

For NMR analysis: a solution of H₂O₂ (2.5 mM) was added in one portion at room temperature to a solution of 4-CP (2.5 mM), MPS (2.5 mM) and Fe(III)-MC6*a (6.25 × 10⁻³ mM) in 50 mM sodium phosphate (pH 6.5), TFE and D₂O (40:50:10 *v/v/v*). The reaction monitoring was performed by acquiring ¹H NMR spectra over time. A confirmation of the identity of BQ was obtained by comparison with the ¹H NMR spectrum of a commercial sample, acquired under the same conditions.

3.2. TON Determination

The turnover number was determined by GC-MS analysis of the reaction, measuring the conversion degree based on the maximal substrate consumption. Following the procedure reported in the previous paragraph, total ion current (TIC) chromatograms were acquired. The peak areas corresponding to the halophenol and MPS were integrated for all reaction times. The conversion degree was calculated using the following equation:

$$\text{Conversion (\%)} = \frac{\left(\frac{A_{\text{sub}}}{A_{\text{I.Std.}}}\right)_0 - \left(\frac{A_{\text{sub}}}{A_{\text{I.Std.}}}\right)_x}{\left(\frac{A_{\text{sub}}}{A_{\text{I.Std.}}}\right)_0} \cdot 100$$

where A_{sub} and $A_{\text{I.Std.}}$ are the peak areas of the substrate and the internal standard, respectively, in the GC-MS TIC chromatogram. The subscript 0 indicates the trace acquired prior to H₂O₂ addition, while the subscript *x* is a specific time during the reaction. Based on the conversion degree, the TON value was calculated as the ratio between the number of converted substrate molecules and the number of catalyst molecules. The mean TON values along with the corresponding standard deviations are reported in Table 1.

3.3. Synthesis of Compounds 1a and 1b

4-Chloro-2-(4-chlorophenoxy)phenol (1a). Compound **1a** was synthesized from 4-chlorocatechol and 4-chlorophenylboronic acid according to the procedure of Suzuki et al. [55,68]. Spectral data of compound **1a** are fully in line with those reported in the literature [68]. ¹H NMR (CDCl₃, 600 MHz), δ: 5.60 (bs, 1H), 6.78 (d, *J* = 3.8 Hz, 1H), 6.83 (dd, *J* = 2.3, 8.6 Hz, 1H), 6.95 (d, *J* = 8.8 Hz, 2H), 7.06 (d, *J* = 2.4 Hz, 1H), and 7.31 (d, *J* = 8.7 Hz, 2H).

5,5'-Dichloro-[1,1'-biphenyl]-2,2'-diol (1b). A solution of 2,2'-biphenol (200 mg, 1.07 mmol), PTSA (450 mg, 2.36 mmol) and NCS (313 mg, 2.36 mmol) in 10 mL of ACN was stirred at room temperature for 16 h. The reaction was quenched with water and the mixture extracted with dichloromethane. The combined organic layers were dried over Na₂SO₄ and concentrated under vacuum. Purification by flash chromatography on silica gel (hexane/ethyl acetate = 9/1) afforded 190 mg (0.43 mmol, 40%) of a white solid. ¹H NMR (ACN-*d*₃, 600 MHz), δ: 6.93 (d, *J* = 8.5 Hz, 2H), 7.15 (bs, 2H), 7.24 (d, *J* = 2.2 Hz, 2H), and 7.26 (dd, *J* = 2.5, 8.5 Hz, 2H). ¹³C NMR (ACN-*d*₃, 100 MHz): 118.6, 125.3, 126.9, 130.0, 131.8, and 153.8 ppm.

3.4. Analysis of Polymerization Products in the Enzyme-Catalyzed 4-CP Oxidation

The polymerization reactions were performed separately using Fe-MC6*a and HRP as catalysts. Compared to previous conditions (Figure 6) [66], higher concentrations of biocatalysts were herein used to enable the full conversion of the starting material: (a) [Fe-MC6*a] = 1.0 × 10⁻² mM; [4-CP] = 2.5 mM; [H₂O₂] = 2.5 mM in 50 mM phosphate buffer (pH 6.5) with 50% TFE (*v/v*) at 25 °C; (b) [HRP] = 1.0 × 10⁻³ mM; [4-CP] = 2.5 mM; [H₂O₂] = 2.5 mM in 100 mM phosphate buffer (pH 6) at 30 °C. In both cases, the reactions were carried out in overall volumes of 10 mL. After 1 h, control HPLC runs indicated that no residual 4-CP was present in both reaction mixtures.

Afterwards, reaction (a) was concentrated under reduced pressure to remove TFE. The resulting suspension was centrifuged; the precipitate was washed several times with water and then lyophilized to obtain a black powder. Analogously, the reaction mixture (b) was centrifuged; the precipitate was washed several times with water and then lyophilized, obtaining a black powder.

MALDI-MS analysis: a suspension of polymerization products obtained by Fe-MC6*a or HRP catalysis (0.5 μ L) in 7:3 ACN:H₂O (*v/v*) was mixed with a 20 mg/mL solution of α -CHCA in 7:3 ACN:H₂O (*v/v*) (0.5 μ L) and deposited onto a metal target plate for MALDI-MS analysis. The MS spectra were acquired in the positive reflectron mode using a mass (*m/z*) range of 200–4000 Da.

FT-IR analysis: a few milligrams of the black powders were placed onto the ATR cell of the FT-IR spectrometer and analyzed.

4. Conclusions

This work represents a further extension of our research aimed at evaluating the catalytic potential of the miniaturized metalloenzyme Fe-MC6*a. The catalytic behavior of Fe-MC6*a toward the oxidation of differently halogenated phenols was herein screened. The complete characterization of the reaction products for the 4-halophenols case study highlighted interesting catalyst performances. Fe-MC6*a catalyzed the selective oxidative dehalogenation of 4-FP into BQ, while the same reaction with 4-CP, 4-BP and 4-IP resulted in the formation of higher molecular weight compounds. After UHPLC, UV-Vis, NMR, MS and IR analyses, we collected strong indications that oligomers based on C-O bonds were selectively formed during 4-CP oxidation. Differently from all natural and artificial metalloenzymes tested so far in the same reaction, Fe-MC6*a thus demonstrated a distinctive enzymatic character, promoting substrate-dependent chemodivergent transformations with a very high selectivity. This peculiarity is well suited for synthetic applications toward complex halophenol-derived synthons. Even though the preferred formation of specific intermediates is supposed to be at the origin of this catalytic behavior, in-depth mechanistic studies, currently under course, are needed to clarify the peculiar role of this catalyst in respect to the natural and artificial metalloenzymes known so far.

Supplementary Materials: The following supporting information can be downloaded at: <https://www.mdpi.com/article/10.3390/ijms24098058/s1>.

Author Contributions: Conceptualization, V.P., F.N. and A.L.; data curation, D.D. and M.D.F.; formal analysis, D.D. and M.D.F.; investigation, D.D. and M.D.F.; methodology, D.D. and M.D.F.; funding acquisition, A.L.; supervision, V.P., A.L. and F.N.; validation, V.P., F.N. and A.L.; writing—original draft, D.D.; and writing—review and editing, A.L. and F.N. All authors have read and agreed to the published version of the manuscript.

Funding: This research was funded by the Italian Ministry of University and Research, PRIN 2020, Project SEA-WAVE 2020BKK3W9 (CUP E69J22001140005).

Data Availability Statement: All relevant data supporting the findings of this study are included in the article and/or in supplementary information files. Data are also available upon request from the corresponding author.

Acknowledgments: We would like to thank Gerardo Zambrano for the preliminary studies on this topic.

Conflicts of Interest: The authors declare no conflict of interest.

References

1. Poulos, T.L. Heme Enzyme Structure and Function. *Chem. Rev.* **2014**, *114*, 3919–3962. [[CrossRef](#)] [[PubMed](#)]
2. Solomon, E.I.; Heppner, D.E.; Johnston, E.M.; Ginsbach, J.W.; Cirera, J.; Qayyum, M.; Kieber-Emmons, M.T.; Kjaergaard, C.H.; Hadt, R.G.; Tian, L. Copper Active Sites in Biology. *Chem. Rev.* **2014**, *114*, 3659–3853. [[CrossRef](#)] [[PubMed](#)]
3. Jasniowski, A.J.; Que, L. Dioxygen Activation by Nonheme Diiron Enzymes: Diverse Dioxygen Adducts, High-Valent Intermediates, and Related Model Complexes. *Chem. Rev.* **2018**, *118*, 2554–2592. [[CrossRef](#)]

4. Nastri, F.; D'Alonzo, D.; Leone, L.; Zambrano, G.; Pavone, V.; Lombardi, A. Engineering Metalloprotein Functions in Designed and Native Scaffolds. *Trends Biochem. Sci.* **2019**, *44*, 1022–1040. [[CrossRef](#)] [[PubMed](#)]
5. Wittwer, M.; Markel, U.; Schiffels, J.; Okuda, J.; Sauer, D.F.; Schwaneberg, U. Engineering and Emerging Applications of Artificial Metalloenzymes with Whole Cells. *Nat. Catal.* **2021**, *4*, 814–827. [[CrossRef](#)]
6. Maglio, O.; Nastri, F.; Lombardi, A. Structural and Functional Aspects of Metal Binding Sites in Natural and Designed Metalloproteins. In *Ionic Interactions in Natural and Synthetic Macromolecules*; Ciferri, A., Perico, A., Eds.; John Wiley & Sons, Inc.: Hoboken, NJ, USA, 2012; pp. 361–450. ISBN 978-1-118-16585-0.
7. Huang, X.; Groves, J.T. Oxygen Activation and Radical Transformations in Heme Proteins and Metalloporphyrins. *Chem. Rev.* **2018**, *118*, 2491–2553. [[CrossRef](#)]
8. Valasatava, Y.; Rosato, A.; Furnham, N.; Thornton, J.M.; Andreini, C. To What Extent Do Structural Changes in Catalytic Metal Sites Affect Enzyme Function? *J. Inorg. Biochem.* **2018**, *179*, 40–53. [[CrossRef](#)]
9. Lu, Y.; Yeung, N.; Sieracki, N.; Marshall, N.M. Design of Functional Metalloproteins. *Nature* **2009**, *460*, 855–862. [[CrossRef](#)]
10. Schwizer, F.; Okamoto, Y.; Heinisch, T.; Gu, Y.; Pellizzoni, M.M.; Lebrun, V.; Reuter, R.; Köhler, V.; Lewis, J.C.; Ward, T.R. Artificial Metalloenzymes: Reaction Scope and Optimization Strategies. *Chem. Rev.* **2018**, *118*, 142–231. [[CrossRef](#)]
11. Nastri, F.; Chino, M.; Maglio, O.; Bhagi-Damodaran, A.; Lu, Y.; Lombardi, A. Design and Engineering of Artificial Oxygen-Activating Metalloenzymes. *Chem. Soc. Rev.* **2016**, *45*, 5020–5054. [[CrossRef](#)]
12. Chino, M.; Leone, L.; Zambrano, G.; Pirro, F.; D'Alonzo, D.; Firpo, V.; Aref, D.; Lista, L.; Maglio, O.; Nastri, F.; et al. Oxidation Catalysis by Iron and Manganese Porphyrins within Enzyme-like Cages. *Biopolymers* **2018**, *109*, e23107. [[CrossRef](#)] [[PubMed](#)]
13. Lombardi, A.; Nastri, F.; Pavone, V. Peptide-Based Heme–Protein Models. *Chem. Rev.* **2001**, *101*, 3165–3190. [[CrossRef](#)] [[PubMed](#)]
14. Lombardi, A.; Pirro, F.; Maglio, O.; Chino, M.; DeGrado, W.F. De Novo Design of Four-Helix Bundle Metalloproteins: One Scaffold, Diverse Reactivities. *Acc. Chem. Res.* **2019**, *52*, 1148–1159. [[CrossRef](#)] [[PubMed](#)]
15. Chalkley, M.J.; Mann, S.I.; DeGrado, W.F. De Novo Metalloprotein Design. *Nat. Rev. Chem.* **2021**, *6*, 31–50. [[CrossRef](#)]
16. Koebke, K.J.; Pinter, T.B.J.; Pitts, W.C.; Pecoraro, V.L. Catalysis and Electron Transfer in De Novo Designed Metalloproteins. *Chem. Rev.* **2022**, *122*, 12046–12109. [[CrossRef](#)]
17. Pirro, F.; Schmidt, N.; Lincoff, J.; Widel, Z.X.; Polizzi, N.F.; Liu, L.; Therien, M.J.; Grabe, M.; Chino, M.; Lombardi, A.; et al. Allosteric Cooperation in a De Novo-Designed Two-Domain Protein. *Proc. Natl. Acad. Sci. USA* **2020**, *117*, 33246–33253. [[CrossRef](#)]
18. Chino, M.; Zhang, S.-Q.; Pirro, F.; Leone, L.; Maglio, O.; Lombardi, A.; DeGrado, W.F. Spectroscopic and Metal Binding Properties of a De Novo Metalloprotein Binding a Tetrazinc Cluster. *Biopolymers* **2018**, *109*, e23339. [[CrossRef](#)]
19. Petrik, I.D.; Liu, J.; Lu, Y. Metalloenzyme Design and Engineering through Strategic Modifications of Native Protein Scaffolds. *Curr. Opin. Chem. Biol.* **2014**, *19*, 67–75. [[CrossRef](#)]
20. Lin, Y.-W. Biodegradation of Aromatic Pollutants by Metalloenzymes: A Structural-Functional-Environmental Perspective. *Coord. Chem. Rev.* **2021**, *434*, 213774. [[CrossRef](#)]
21. Renata, H.; Wang, Z.J.; Arnold, F.H. Expanding the Enzyme Universe: Accessing Non-Natural Reactions by Mechanism-Guided Directed Evolution. *Angew. Chem. Int. Ed.* **2015**, *54*, 3351–3367. [[CrossRef](#)]
22. Bunzel, H.A.; Anderson, J.L.R.; Mulholland, A.J. Designing Better Enzymes: Insights from Directed Evolution. *Curr. Opin. Struct. Biol.* **2021**, *67*, 212–218. [[CrossRef](#)]
23. Zhu, J.; Avakyan, N.; Kakkis, A.; Hoffnagle, A.M.; Han, K.; Li, Y.; Zhang, Z.; Choi, T.S.; Na, Y.; Yu, C.-J.; et al. Protein Assembly by Design. *Chem. Rev.* **2021**, *121*, 13701–13796. [[CrossRef](#)]
24. Eberly, J.O.; Ely, R.L. Thermotolerant Hydrogenases: Biological Diversity, Properties, and Biotechnological Applications. *Crit. Rev. Microbiol.* **2008**, *34*, 117–130. [[CrossRef](#)]
25. Pineda-Knauseder, A.J.; Vargas, D.A.; Fasan, R. Organic Solvent Stability and Long-term Storage of Myoglobin-based Carbene Transfer Biocatalysts. *Biotechnol. Appl. Biochem.* **2020**, *67*, 516–526. [[CrossRef](#)]
26. Hindson, S.A.; Bunzel, H.A.; Frank, B.; Svistunenko, D.A.; Williams, C.; van der Kamp, M.W.; Mulholland, A.J.; Pudney, C.R.; Anderson, J.L.R. Rigidifying a De Novo Enzyme Increases Activity and Induces a Negative Activation Heat Capacity. *ACS Catal.* **2021**, *11*, 11532–11541. [[CrossRef](#)]
27. Chen, K.; Arnold, F.H. Engineering New Catalytic Activities in Enzymes. *Nat. Catal.* **2020**, *3*, 203–213. [[CrossRef](#)]
28. Jenkins, J.M.X.; Noble, C.E.M.; Grayson, K.J.; Mulholland, A.J.; Anderson, J.L.R. Substrate Promiscuity of a de Novo Designed Peroxidase. *J. Inorg. Biochem.* **2021**, *217*, 111370. [[CrossRef](#)]
29. Leone, L.; Chino, M.; Nastri, F.; Maglio, O.; Pavone, V.; Lombardi, A. Mimochrome, a Metalloporphyrin-based Catalytic Swiss Knife. *Biotechnol. Appl. Biochem.* **2020**, *67*, 495–515. [[CrossRef](#)]
30. Di Costanzo, L.; Geremia, S.; Randaccio, L.; Nastri, F.; Maglio, O.; Lombardi, A.; Pavone, V. Miniaturized Heme Proteins: Crystal Structure of Co(III)-Mimochrome IV. *J. Biol. Inorg. Chem.* **2004**, *9*, 1017–1027. [[CrossRef](#)]
31. Firpo, V.; Le, J.M.; Pavone, V.; Lombardi, A.; Bren, K.L. Hydrogen Evolution from Water Catalyzed by Cobalt-Mimochrome VI^a, a Synthetic Mini-Protein. *Chem. Sci.* **2018**, *9*, 8582–8589. [[CrossRef](#)]
32. Le, J.M.; Alachouzos, G.; Chino, M.; Frontier, A.J.; Lombardi, A.; Bren, K.L. Tuning Mechanism through Buffer Dependence of Hydrogen Evolution Catalyzed by a Cobalt Mini-Enzyme. *Biochemistry* **2020**, *59*, 1289–1297. [[CrossRef](#)] [[PubMed](#)]
33. Edwards, E.H.; Le, J.M.; Salamatian, A.A.; Peluso, N.L.; Leone, L.; Lombardi, A.; Bren, K.L. A Cobalt Mimochrome for Photochemical Hydrogen Evolution from Neutral Water. *J. Inorg. Biochem.* **2022**, *230*, 111753. [[CrossRef](#)] [[PubMed](#)]

34. Leone, L.; D'Alonzo, D.; Balland, V.; Zambrano, G.; Chino, M.; Natri, F.; Maglio, O.; Pavone, V.; Lombardi, A. Mn-Mimochrome VI^a: An Artificial Metalloenzyme With Peroxygenase Activity. *Front. Chem.* **2018**, *6*, 590. [CrossRef] [PubMed]
35. Leone, L.; D'Alonzo, D.; Maglio, O.; Pavone, V.; Natri, F.; Lombardi, A. Highly Selective Indole Oxidation Catalyzed by a Mn-Containing Artificial Mini-Enzyme. *ACS Catal.* **2021**, *11*, 9407–9417. [CrossRef]
36. Caserta, G.; Chino, M.; Firpo, V.; Zambrano, G.; Leone, L.; D'Alonzo, D.; Natri, F.; Maglio, O.; Pavone, V.; Lombardi, A. Enhancement of Peroxidase Activity in Artificial Mimochrome VI Catalysts through Rational Design. *ChemBioChem* **2018**, *19*, 1823–1826. [CrossRef]
37. Zambrano, G.; Natri, F.; Pavone, V.; Lombardi, A.; Chino, M. Use of an Artificial Miniaturized Enzyme in Hydrogen Peroxide Detection by Chemiluminescence. *Sensors* **2020**, *20*, 3793. [CrossRef]
38. Zambrano, G.; Sekretareva, A.; D'Alonzo, D.; Leone, L.; Pavone, V.; Lombardi, A.; Natri, F. Oxidative Dehalogenation of Trichlorophenol Catalyzed by a Promiscuous Artificial Heme-Enzyme. *RSC Adv.* **2022**, *12*, 12947–12956. [CrossRef]
39. Garba, Z.N.; Zhou, W.; Lawan, I.; Xiao, W.; Zhang, M.; Wang, L.; Chen, L.; Yuan, Z. An Overview of Chlorophenols as Contaminants and Their Removal from Wastewater by Adsorption: A Review. *J. Environ. Manag.* **2019**, *241*, 59–75. [CrossRef]
40. Mercier, C.; Youmans, P. 4-Fluorophenol: A Key Intermediate for Agrochemicals and Pharmaceuticals. In *Industrial Chemistry Library*; Elsevier: Amsterdam, The Netherlands, 1996; Volume 8, pp. 293–300. ISBN 978-0-444-82434-9.
41. Hamid, M. Khalil-ur-Rehman Potential Applications of Peroxidases. *Food Chem.* **2009**, *115*, 1177–1186. [CrossRef]
42. Osborne, R.L.; Coggins, M.K.; Walla, M.; Dawson, J.H. Horse Heart Myoglobin Catalyzes the H₂O₂ -Dependent Oxidative Dehalogenation of Chlorophenols to DNA-Binding Radicals and Quinones. *Biochemistry* **2007**, *46*, 9823–9829. [CrossRef]
43. Franzen, S.; Thompson, M.K.; Ghiladi, R.A. The Dehaloperoxidase Paradox. *Biochim. Biophys. Acta BBA—Proteins Proteom.* **2012**, *1824*, 578–588. [CrossRef]
44. Wang, Y.; Liu, A. Carbon–Fluorine Bond Cleavage Mediated by Metalloenzymes. *Chem. Soc. Rev.* **2020**, *49*, 4906–4925. [CrossRef]
45. Osborne, R.L.; Raner, G.M.; Hager, L.P.; Dawson, J.H. C. *Fumago* Chloroperoxidase Is Also a Dehaloperoxidase: Oxidative Dehalogenation of Halophenols. *J. Am. Chem. Soc.* **2006**, *128*, 1036–1037. [CrossRef]
46. Murphy, C.D. Fluorophenol Oxidation by a Fungal Chloroperoxidase. *Biotechnol. Lett.* **2006**, *29*, 45–49. [CrossRef]
47. Pirzad, R.; Newman, J.D.; Dowman, A.A.; Cowell, D.C. Horseradish Peroxidase Assay—Radical Inactivation or Substrate Inhibition? Revision of the Catalytic Sequence Following Mass Spectral Evidence. *Analyst* **1994**, *119*, 213–218. [CrossRef]
48. Kozuch, S.; Martin, J.M.L. “Turning Over” Definitions in Catalytic Cycles. *ACS Catal.* **2012**, *2*, 2787–2794. [CrossRef]
49. Chen, Y.P.; Woodin, S.A.; Lincoln, D.E.; Lovell, C.R. An Unusual Dehalogenating Peroxidase from the Marine Terebellid Polychaete *Amphitrite ornata*. *J. Biol. Chem.* **1996**, *271*, 4609–4612. [CrossRef]
50. De Serrano, V.; Franzen, S. Structural Evidence for Stabilization of Inhibitor Binding by a Protein Cavity in the Dehaloperoxidase-Hemoglobin from *Amphitrite ornata*. *Biopolymers* **2012**, *98*, 27–35. [CrossRef]
51. Thompson, M.K.; Davis, M.F.; de Serrano, V.; Nicoletti, F.P.; Howes, B.D.; Smulevich, G.; Franzen, S. Internal Binding of Halogenated Phenols in Dehaloperoxidase-Hemoglobin Inhibits Peroxidase Function. *Biophys. J.* **2010**, *99*, 1586–1595. [CrossRef]
52. Vatsis, K.P.; Coon, M.J. Ipso-Substitution by Cytochrome P450 with Conversion of *p*-Hydroxybenzene Derivatives to Hydroquinone: Evidence for Hydroperoxo-Iron As the Active Oxygen Species. *Arch. Biochem. Biophys.* **2002**, *397*, 119–129. [CrossRef]
53. Harkey, A.; Kim, H.-J.; Kandagatla, S.; Raner, G.M. Defluorination of 4-Fluorophenol by Cytochrome P450BM3-F87G: Activation by Long Chain Fatty Aldehydes. *Biotechnol. Lett.* **2012**, *34*, 1725–1731. [CrossRef] [PubMed]
54. Osman, A.M.; Boeren, S.; Veeger, C.; Rietjens, I.M.C.M. MP8-Dependent Oxidative Dehalogenation: Evidence for the Direct Formation of 1,4-Benzoquinone from 4-Fluorophenol by a Peroxidase-Type of Reaction Pathway. *Chem. Biol. Interact.* **1997**, *104*, 147–164. [CrossRef] [PubMed]
55. Evans, D.A.; Katz, J.L.; West, T.R. Synthesis of Diaryl Ethers through the Copper-Promoted Arylation of Phenols with Arylboronic Acids. An Expedient Synthesis of Thyroxine. *Tetrahedron Lett.* **1998**, *39*, 2937–2940. [CrossRef]
56. Bentley, K.W.; Joyce, L.A.; Sherer, E.C.; Sheng, H.; Wolf, C.; Welch, C.J. Antenna Biphenols: Development of Extended Wavelength Chiroptical Reporters. *J. Org. Chem.* **2016**, *81*, 1185–1191. [CrossRef] [PubMed]
57. Osborne, R.L.; Coggins, M.K.; Raner, G.M.; Walla, M.; Dawson, J.H. The Mechanism of Oxidative Halophenol Dehalogenation by *Amphitrite ornata* Dehaloperoxidase Is Initiated by H₂O₂ Binding and Involves Two Consecutive One-Electron Steps: Role of Ferryl Intermediates. *Biochemistry* **2009**, *48*, 4231–4238. [CrossRef]
58. Belyea, J.; Gilvey, L.B.; Davis, M.F.; Godek, M.; Sit, T.L.; Lommel, S.A.; Franzen, S. Enzyme Function of the Globin Dehaloperoxidase from *Amphitrite ornata* is Activated by Substrate Binding. *Biochemistry* **2005**, *44*, 15637–15644. [CrossRef]
59. NIST/EPA Gas-Phase Infrared Database. Available online: <https://webbook.nist.gov/cgi/cbook.cgi?ID=C106514&Mask=80#IR-Spec> (accessed on 27 April 2023).
60. Nicell, J.A.; Bewtra, J.K.; Taylor, K.E.; Biswas, N.; St Pierre, C. Enzyme Catalyzed Polymerization and Precipitation of Aromatic Compounds from Wastewater. *Water Sci. Technol.* **1992**, *25*, 157–164. [CrossRef]
61. Nicell, J.A.; Bewtra, J.K.; Biswas, N.; St Pierre, C.C.; Taylor, K.E. Enzyme Catalyzed Polymerization and Precipitation of Aromatic Compounds from Aqueous Solution. *Can. J. Civ. Eng.* **1993**, *20*, 725–735. [CrossRef]
62. Reihmann, M.; Ritter, H. Synthesis of Phenol Polymers Using Peroxidases. In *Enzyme-Catalyzed Synthesis of Polymers*; Kobayashi, S., Ritter, H., Kaplan, D., Eds.; Advances in Polymer Science; Springer: Berlin/Heidelberg, Germany, 2006; Volume 194, pp. 1–49. ISBN 978-3-540-29212-8.

63. Vojinović, V.; Carvalho, R.H.; Lemos, F.; Cabral, J.M.S.; Fonseca, L.P.; Ferreira, B.S. Kinetics of Soluble and Immobilized Horseradish Peroxidase-Mediated Oxidation of Phenolic Compounds. *Biochem. Eng. J.* **2007**, *35*, 126–135. [[CrossRef](#)]
64. Sarno, M.; Iuliano, M. New Nano-Biocatalyst for 4-Chlorophenols Removal from Wastewater. *Mater. Today Proc.* **2020**, *20*, 74–81. [[CrossRef](#)]
65. Lu, Y.; Zhang, T.; Zhang, Y.-X.; Sang, X.-J.; Su, F.; Zhu, Z.-M.; Zhang, L.-C. A POM-Based Copper-Coordination Polymer Crystal Material for Phenolic Compound Degradation by Immobilizing Horseradish Peroxidase. *Dalton Trans.* **2021**, *50*, 15198–15209. [[CrossRef](#)]
66. Yamada, K.; Shibuya, T.; Noda, M.; Uchiyama, N.; Kashiwada, A.; Matsuda, K.; Hirata, M. Influence of Position of Substituent Groups on Removal of Chlorophenols and Cresols by Horseradish Peroxidase and Determination of Optimum Conditions. *Biosci. Biotechnol. Biochem.* **2007**, *71*, 2503–2510. [[CrossRef](#)]
67. Sun, S.; Sono, M.; Du, J.; Dawson, J.H. Evidence of the direct involvement of the substrate TCP radical in functional switching from oxyferrous O₂ carrier to ferric peroxidase in the dual-function hemoglobin/dehaloperoxidase from *Amphitrite ornata*. *Biochemistry* **2014**, *53*, 4956–4969. [[CrossRef](#)]
68. Suzuki, Y.; Nakamura, M.; Otsuka, Y.; Suzuki, N.; Ohyama, K.; Kawakami, T.; Sato, K.; Kajita, S.; Hishiyama, S.; Fujii, T.; et al. Novel Enzymatic Activity of Cell Free Extract from Thermophilic *Geobacillus* Sp. UZO 3 Catalyzes Reductive Cleavage of Diaryl Ether Bonds of 2,7-Dichlorodibenzo-*p*-Dioxin. *Chemosphere* **2011**, *83*, 868–872. [[CrossRef](#)]

Disclaimer/Publisher’s Note: The statements, opinions and data contained in all publications are solely those of the individual author(s) and contributor(s) and not of MDPI and/or the editor(s). MDPI and/or the editor(s) disclaim responsibility for any injury to people or property resulting from any ideas, methods, instructions or products referred to in the content.